Realization of ordered magnetic skyrmions in thin films at ambient conditions

Ryan D. Desautels, Lisa DeBeer-Schmitt, Sergio A. Montoya, Julie A. Borchers, Soong-Geun Je, Nan Tang, Mi-Young Im, Michael R. Fitzsimmons, Eric E. Fullerton, and Dustin A. Gilbert

Phys. Rev. Materials **3**, 104406 — Published 10 October 2019

DOI: 10.1103/PhysRevMaterials.3.104406

Realization of Ordered Magnetic Skyrmions in Thin Films at Ambient Conditions

Ryan D. Desautels* and Lisa DeBeer-Schmitt†

Neutron Scattering Division, Oak Ridge National Laboratory, Oak Ridge, Tennessee 37831, USA

Sergio A. Montoya

Naval Information Warfare Center Pacific, San Diego, CA 92152, USA

Julie A. Borchers

NIST Center for Neutron Research, National Institute of Standards and Technology, Gaithersburg, MD 20899, USA

Soong-Geun Je

Center for X-ray Optics, Lawrence Berkeley National Laboratory, Berkeley, CA 94270, USA

Nan Tang

Department of Materials Science and Engineering, University of Tennessee, Knoxville, TN 37996, USA

Mi-Young Im

Center for X-ray Optics, Lawrence Berkeley National Laboratory, Berkeley, CA 94270, USA, and School of Materials Science and Engineering, Ulsan National Institute of Science and Technology, Ulsan, Republic of Korea

Michael R. Fitzsimmons

Neutron Scattering Division, Oak Ridge National Laboratory, Oak Ridge, Tennessee 37831, USA and Department of Physics and Astronomy, University of Tennessee, Knoxville TN 37996, USA

Eric E. Fullerton

Center for Memory and Recording Research, University of California, San Diego, La Jolla, CA 92093, USA

Dustin A. Gilbert

NIST Center for Neutron Research,

National Institute of Standards and Technology, Gaithersburg,

MD 20899, USA and Department of Materials Science and Engineering,

University of Tennessee, Knoxville, TN 37996, USA

(Dated: September 19, 2019)

Abstract

Magnetic skyrmions have captivated physicists due to their topological nature and novel physical properties. In addition, skyrmions hold significant promise for future information technologies. A key barrier to realizing skyrmion-based devices has been stabilizing these spin structures under ambient conditions. In this manuscript, we demonstrate that the tunable magnetic properties of amorphous Fe/Gd mulitlayers enable the formation of skyrmion lattices which are stable over a large temperature and magnetic field parameter space, including room temperature and zero magnetic field. These skyrmions, having a hybrid nature displaying both Bloch-type and Néel-type characteristics, are stabilized by dipolar interactions rather than Dzyaloshinskii-Moriya interactions, typically considered a requirement for the generation of skyrmions. Small angle neutron scattering was used in combination with soft X-ray microscopy to provide a unique, multi-scale probe of the local and long-range order of these structures. The hexagonal lattice seen in SANS results from the hybrid skyrmion picture were corroborated with micromagnetic simulations. These results identify a pathway to engineer controllable skyrmion phases in thin film geometries which are stable at ambient conditions.

INTRODUCTION

Skyrmions have emerged as a promising approach to realize next-generation, ultra-low power memory and logic devices[1–4]. The small spatial size of these magnetic structures (near atomic scale[5]) coupled with their relative ease of current induced mobility[6] and topologically enhanced stability[1], make these chiral spin textures among the most exciting emerging spintronic technologies. These advantages are present within skyrmions due to their spin configuration and hence are independent of the stabalizing mechanism. The ability to stabilize skyrmion structures in environments relevant to consumer technologies remains a challenging barrier to realizing skyrmion-based devices today. In prototypical bulk skyrmion materials (e.g. MnSi, (Fe,Co)Si, Cu_2OSeO_3, FeGe), the stability window tends to be below room temperature[4, 7], and always in finite magnetic fields[8, 9]. Progress, particularly in manipulating interfacial Dzyaloshinskii-Moriya (DM) interactions[10], has allowed

* These two authors contributed equally

† These two authors contributed equally; debeerschmlm@ornl.gov

researchers to make excellent advances in achieving room-temperature stability.[4, 11] However, comparably few approaches have been demonstrated which can stabilize skyrmions at zero applied magnetic field, including rapid quenching[8, 12], pulsed electrical currents[13], geometric confinement[14, 15], or pinning the skyrmions with nanostructures[16, 17]. These approaches place restrictions on the skyrmion system, limiting both fundamental research and eventual device architectures. Removing the requisite magnetic field, especially at room temperature, is crucial to the integration of skyrmions into spintronic architectures.[18].

We demonstrate the formation of an ordered magnetic skyrmion lattice in amorphous Fe/Gd thin-film multilayers stabilized through dipolar interactions rather than DM interactions. These skyrmions have been suggested to be dipole stabalized[19, 20], but may also have contributions from random anisotropy (RA) specific to amorphous and nanocrystalline systems[21]. Utilizing a straight forward magnetic field sequence (discussed in the methods section), the labyrinthine domains typically present at remanence are ordered into artificial stripe domains, analogous to traditional B20-structured skyrmion materials[7]. The skyrmion regime is accessed by increasing the magnetic field from the stripe state, breaking up the stripes and precipitating arrays of ordered skyrmions with long-range orientation. Once generated, these dipole-stabilized skyrmions[19, 20] are stable over a field range from 200 mT to -55 mT, including zero magnetic field, and a temperature range from 10 K to 320 K, which moves towards the parameter space of consumer technologies. Unlike traditional skyrmion systems which are stabilized by DM interactions, dipole-stabilized skyrmions possess no symmetry breaking in the in-plane circularity and thus both chiralities can be realized. However, this is not the case at the surfaces of the skyrmion columns. Specifically, these dipole-stabilized skyrmions possess flux-closure domains at the top and bottom surfaces, which have a structure analogous to Néel-type skyrmions. The orientation of the Néel caps follow the in-plane component of the dipole fields, and thus possess a chirality which is uniform for all of the skyrmions with a common core orientation[22], as shown in Figure 1. Further the chirality of the top surface is opposite to the chirality of the bottom surface; in Figure 1, the chirality on the top surface is radially outward, while the bottoms surface is radially inward. Previous Lortenz transmission electron microscopy (LTEM) results and micromagnetic simulations have shown that these skyrmions possess a Bloch-type structure at the equatorial band[19, 20], with the moments wrapping along the azimuthal direction. The dipole field in this region is vertical, along the film normal, with no in-plane component, and

thus does not define the chirality since the moments are orthogonal to the dipole fields. Indeed, the LTEM results confirm the random chirality of the Bloch regions. The combination of the Néel caps on the top and bottom, and the Bloch-type winding at the equatorial belt constitutes a hybrid skyrmion structure[20, 23, 24]. These dipole skyrmions form an ordered lattice stabilized by the mutual repulsion of these caps. The dipole-stabilized skyrmions in our Fe/Gd system open up a new rich playground of physical phenomena and emergent technologies to explore[4].

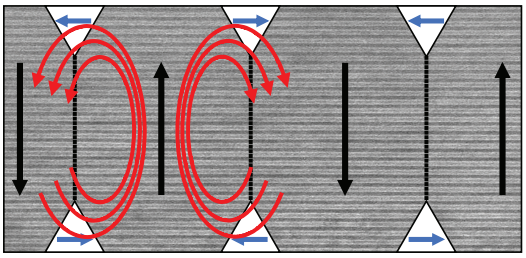

FIG. 1. Cross sectional view of the multilayer film, with flux closure domains illustratively included at the top and bottom surfaces. The chirality of the domains (blue) follows the magnetic dipole fields (red). In the middle of the film, the moments orient in-plane, enclosing the core of the skyrmion as observed with LTEM[19, 20]. The dipole fields are along the film normal direction at the film's center, orthogonal to the spins, and thus the dipole fields do not define a chirality. Since there is no other symmetry breaking mechanism (e.g. DMI or geometry[25]), the moments at the equatorial band have no net chirality, again consistent with the LTEM.

METHODS

The Fe/Gd multilayer films were deposited on 1 cm^2 (001) Si substrates witgh native SiO_2 layer by DC magnetron sputtering. Growth was performed at room temperature in an ultrahigh vacuum after which a 3 mTorr (1 Torr = 133 Pa) argon gas environment was added during the deposition process[19, 20]. The multilayer films were grown by depositing alternating layers of Fe and Gd until the desired number of layers was achieved. In all cases, 5 nm tantalum seed and capping (to prevent oxidation) layers were used. This structure of the film is illustrated in Figure 2a, and a photograph of the sample mounted in the instrument in Figure 2b.

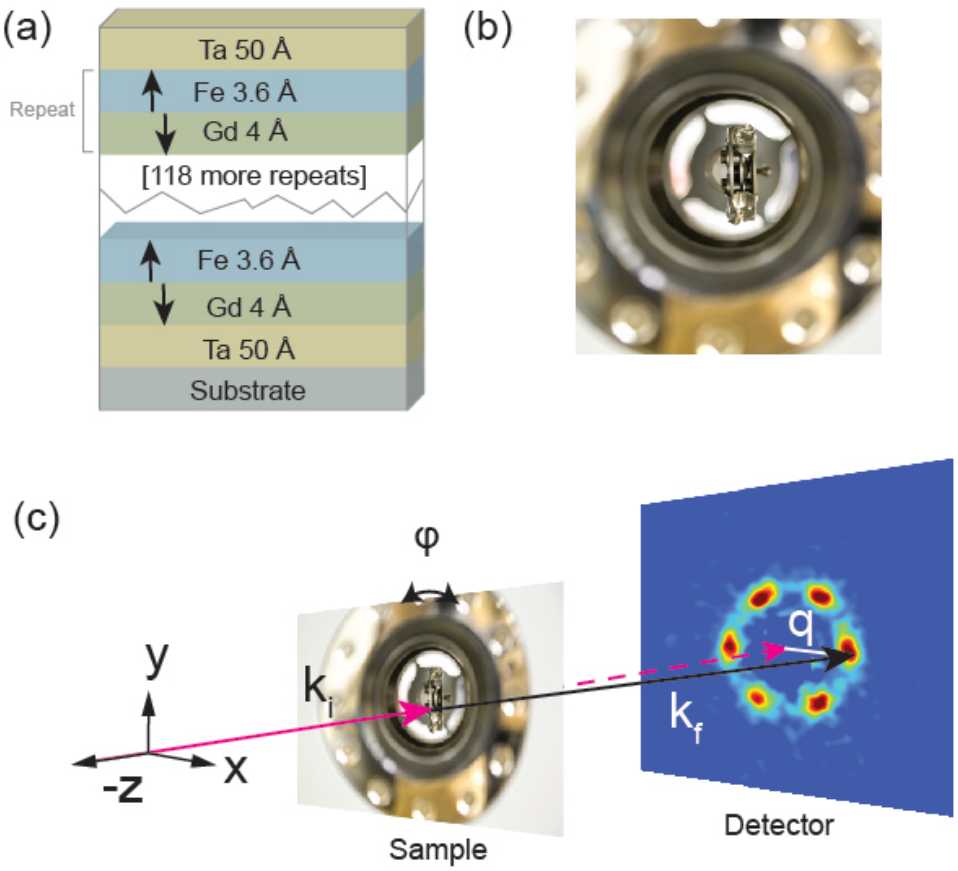

FIG. 2. (a) Schematic depiction of the 120 repeat Fe/Gd bilayer stack. This stack contains individual Fe layers 3.6 Å thick and Gd layers 4.0 Å thick. (b) Photograph of the [(Fe(3.6 Å)/Gd(4.0 Å)]×120 film stack mounted inside the film holder. The films are held within the bore of a 5 T magnet at room temperature. The sample normal, neutron beam and magnetic field are left-to-right in the image. Image credit: Genevieve Martin/ORNL (c) Schematic diagram of the 2D SANS experimental setup. The incoming neutrons are co-aligned with the films' surface normal and the applied magnetic field. The resulting SANS image is of the wave vector transfer in the q_y and q_x directions (in the detector plane).

Two-dimensional small angle neutron scattering (2D SANS) experiments were initially performed at the GP-SANS beam line at Oak Ridge National Laboratory's (ORNL) High Flux Isotope Reactor (HFIR)[26, 27]. These experiments were performed at room temperature and varying the magnetic field using a 5 T horizontal open bore dry cryogenic superconducting magnet, with the magnetic field aligned parallel to the neutron beam (Figure 2c). The SANS instrument was configured to use 16 Å neutrons ($\Delta\lambda/\lambda = 0.13$) with a detector

distance of 19.2 m on a co-linear aligned stack of 12 films of [(Fe(3.6 Å) / Gd(4.0 Å)]×120). This sample holder ensures that the films remain aligned co-linearly and restricts any in-plane rotation/slipping of the film stack. An 8 mm-diameter aperture was used to fully illuminate the films in the beam. The temperature dependent measurements were performed using the Very Small Angle Neutron Scattering (VSANS) beam line at the National Institute for Standards and Technology (NIST) wit 14 Å neutrons, a water cooled resistive electromagnet, and a closed-cycle refrigeration system.

The artificially aligned stripe domains were stabilized by rotating the sample about the x-axis (out of the figure plane in Figure 2c) by $\approx 45^\circ$ and applying a saturating field of $\mu_0 H = 500$ mT. Typically, measurements are performed with the magnetic field along the film normal direction; reducing the field from saturation would nucleate randomly oriented labyrinth domains. By tilting the sample, the in-plane projection of the field breaks the symmetry and orders the domains as stripe domains, oriented along the in-plane field component direction. After removing the magnetic field, the sample was rotated to its original configuration, with the films' normal along the direction of the neutron beam, (Figure 2c) for all the SANS measurements. After saturating of the sample with field normal to the film, it will return to the labyrinth stripe domain phase with no in-plane orientation of the stripes [20].

X-ray microscopy images were captured on BL 6.1.2 at the Advanced Light Source. Images were collected in transmission mode using full-field soft X-ray microscopy along the Fe L3 (708 eV) absorption edge. To achieve X-ray transmission, the samples were grown on SiN membrane windows.

Micromagnetic simulations were performed using the Object Oriented Micromagnetic Framework (OOMMF)[28] using a saturation magnetization of 8×10^5 kA/m, exchange stiffness of 1×10^{-11} J/m, and uniaxial anisotropy of 200×10^3 J/m^3; dipole interactions were included but no DM interaction. Stability simulations were performed at $H = 0$ T. The skyrmion size accurately reproduced the experimental results, with diameters of ≈200 nm.

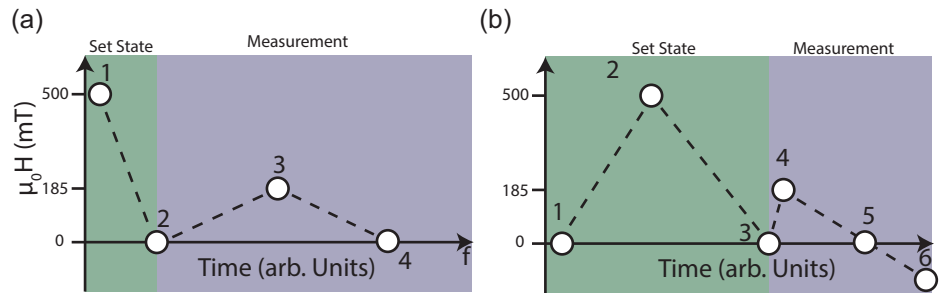

FIG. 3. (**a**) Field sequence to establish the disordered closed packed skyrmion lattice: (1) a saturating field of $\mu_0 H = 500$ mT applied normal to the film, (2) the remanent state ($\mu_0 H = 0$ mT), (3) the skyrmion state with a field applied along the film's normal ($\mu_0 H = 185$ mT) and (4) back to remanence. (**b**) Field sequence to establish the ordered hexagonal skyrmion lattice: (1) films initially at remanence are rotated by ∼45° about the x-axis (Figure 2c), (2) a saturating field of $\mu_0 H = 500$ mT applied in this rotated configuration, (3) films are rotated back to their original configuration in zero applied magnetic field and the artificial stripe domain is measured, (4) the skyrmion state with a field applied along the film's normal ($\mu_0 H = 185$ mT), (5) back to remenenace and (6) continuing to ramp the field towards negative saturation.

RESULTS AND DISCUSSION

SANS measurements were performed on multilayer thin-films of [(Fe(3.6 Å) / Gd(4.0 Å)]×120 oriented with the film normal parallel to the incoming neutron beam and external magnetic field. At remanence, the domains coalesced into long interwoven 'worm-like' structures (labyrinthine domains) with similar widths (illustrated in the inset of Figure 4a)[19, 20]. The Fourier transform of these disordered domains defines the small angle neutron scattering (SANS) pattern[29], and was observed to be a ring (Figure 4a), as expected. Increasing the applied field from remanence to $\mu_0 H = 185$ mT, the disordered labyrinthine domains break apart to form magnetic skyrmions that locally arrange to form closed packed lattices with ≈20 skyrmions, as determined from the X-ray images(Figures 4d and S1), but the domains do not possess a common orientation of the lattice[20], e.g. the domains are rotationally disordered. The disorder is likely a result of the precursor labyrinthe state. While each domain would contribute a hexagonal feature to the SANS pattern, the measured pattern is the sum of all these domains, Figure 4b. One may notice that both the labyrinth and skyrmion phases (Figure 4a and b) form a ring feature, confirming that each phase possesses

local order but no orientation, and indicating the approximate equidistant spacing of the skyrmions and labyrinth domains. Consequently, the two phases are indistinguishable by SANS; intensity differences are a result of variations in the scattering structure and form factor and cannot be used as unique identifiers.

The existence of ordered skyrmion lattices is not expected in the RA model[21], but is likely to form in the dipole model - due to their repulsive interactions. Each of the individual textures resulting from the dissolution of the labyrinthine domains have been reported as having an azimuthally wound, closed loop boundary and antiparallel core and perimeter (Figure 1) characteristic of a Bloch skyrmion. The integrated solid angle of these structures - defining their topological charge - can be unity, making them homotopically equivalent to skyrmions observed in traditional B20 materials[7] or 3d-5d multilayers[10]. One distinction of the skyrmions in this work compared to traditional skyrmion systems is that they are not stabilized by the DM interaction. The likely stabilizing mechanism is dipole interactions between the skyrmion core and the surrounding (antiparallel) matrix; the RA mechanism is expected to play a small role here due to the absence of orbital momentum in the gadolinium[30], which results in minimal magnetocrystalline anisotropy. Neither of these mechanisms have geometric symmetry-breaking, as the DM interaction does, and thus there is no net chirality in the lattice; the two chiral states are energetically degenerate and thus 'writing' to the chirality for data storage applications could be achieved in this system.

Reducing the field back towards remanence, a change in the q-radius is also seen in the patterns for different fields, indicating that the lattice periodicity changes (not shown) but does not affect the ring structure observed in SANS. However, using soft X-ray microscopy(Figure 4d) one can see the skyrmions continue to be present at zero applied field. Calculating the Fast Fourier transform (FFT) of the X-ray image, Figure 4d inset, shows a ring - the observed truncation of the FFT leads to artifact on the Cartesian axes and does not correspond to any experimental feature. Soft X-ray microscopy provides a local, real-space image to distinguish between the disordered skyrmion state and labyrinth states that look the same with SANS. SANS is an ensemble average and is related to the Fourier transform of the X-ray data. More X-ray images are presented in the Supplemental Materials in Figure S1 which show the field evolution of the skyrmions in the disordered state[31].

Comparing the skyrmions and labyrinthine domain structure reported here to traditional skyrmion materials, the skyrmion phase in B20 thin-films is bounded by chiral stripe

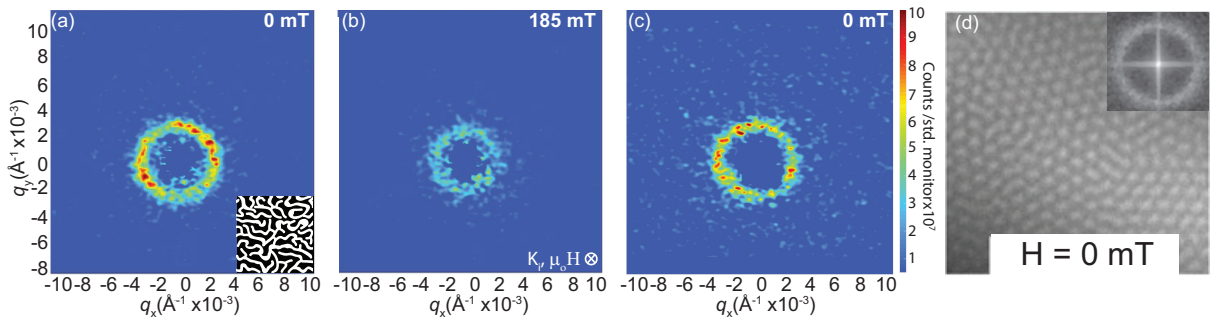

FIG. 4. Disordered skyrmions in a continuous amorphous thin film. Initially, the [(Fe(3.6 Å) / Gd(4.0 Å)]×120 film was saturated with a field parallel to the incoming neutrons and normal to the films (see Figure 3a). The inset is a illustration of the labyrthine domains. SANS patterns collected at; (**a**) remanance ($\mu_0 H = 0$ T), (**b**) within the disordered skyrmion state ($\mu_0 H = 185$ mT), (**c**) and back at remanence from the disordered skyrmion state. (**d**) Soft X-ray microscopy images taken at $\mu_0 H = 0$ T, after analogous field preparation.

phases[7] at lower fields and temperatures[32]. We propose that by promoting order within the labyrinth structure, an artificial stripe phase can be realized which mimics the stripe phase in the traditional materials, and the resultant skyrmions may form with long-range coherent order. Ordering of the labyrinthine domains was accomplished by first rotating the sample's surface normal by $\approx 45°$ relative to the magnetic field (Figure 3b) after which a saturating field (500 mT) was applied, then the field was reduced to remanence. Saturation of the sample in the rotated geometry induces an in-plane projection of the field which breaks the symmetry and orders the labyrinthine domains into oriented stripe domains, see illustrations of the state in inset of Figure 5a. The sample was then rotated back to its original orientation - with the surface normal parallel to the neutrons and magnetic field - and the SANS pattern was measured. The SANS measurement shows two bright peaks along the axis of the film's rotation (Figure 5a), indicating that the labyrinthine domains are ordered, with stripes forming parallel to the in-plane field projection during the saturation sequence.

Increasing the magnetic field from remanence to $\mu_0 H = 185$ mT, applied along the film's surface normal, the SANS pattern evolves from two peaks located on the horizontal (q_x) axis (which also was the axis of rotation) to six peaks located at 60° increments. Reducing the

magnetic field to $\mu_0 H = 0$ mT, the hexagonal pattern is unchanged (Figure 5b). The 6-fold pattern is widely associated with the skyrmion phase and, compared to the ring pattern in Figure 4b and c, indicates that the skyrmions form hexagonally packed arrays with long range order and orientation. This ordering is expected to occur by setting one of the nearest neighbor axes of the emergent hexagonal skyrmion lattice with the stripe domain orientation, while the other two axes orient to minimize the skyrmion-skyrmion repulsive interaction.

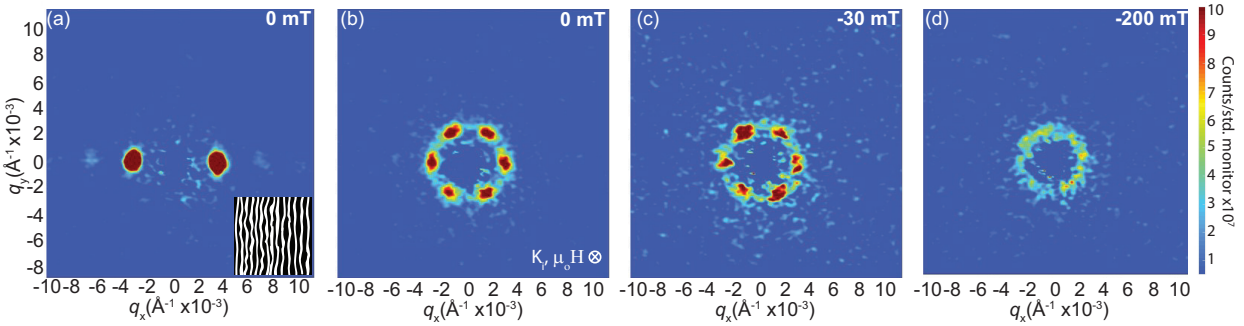

FIG. 5. SANS pattern at sequential fields for [(Fe(3.6 Å) / Gd(4.0 Å)]×120. The sample was saturated in the rotated geometry (Figure 3b) then the field reduced to remanence, then rotated to their original orientation. (**a**) SANS pattern showing two peaks indicating a well-ordered stripe domain structure. The inset is an illustration of the artificially ordered stripe phase. The out-of-plane magnetic field was increased to $\mu_0 H = 185$ mT (not shown). SANS patterns were measured as the magnetic field was reduced towards negative saturation, with measurements shown at (**b**) $\mu_0 H = 0$ T (skyrmion phase), (**c**) $\mu_0 H =$ -30 mT, (**d**) $\mu_0 H =$ -200 mT.

At $\mu_0 H = 0$ (Figure 5b) the SANS feature appears at $|q| = 0.0025(8)$ Å^{-1}, indicating a skyrmion center-to-center separation of 230 nm; this value gives the upper limit to the skyrmion diameter. The lattice's field stability was determined by reducing the out-of-plane magnetic field towards negative saturation (Figure 5b-d). As the magnetic field was reduced from remanence ($H = 0$) to -30 mT (Figure 5c), two peaks become stronger (upper left and lower right), indicating the re-emergence of a co-existing stripe domain phase, in agreement with X-ray microscopy images (see Supplemental Figure S1). The new stripe phase was rotated by 60° relative to the initial orientation in Figure 5c. The difference in orientation may be due to a slight misalignment of the sample with respect the field in the y-axis (Figure 2c) which would give a small in-plane component in that direction, or subtle

texturing within the film. Approaching saturation, the SANS pattern becomes a broad ring of scattering, shown in Figure 5d, suggesting a nearly complete loss of macroscopic order. After achieving magnetic saturation, the SANS pattern collapses to $q = 0$, *i.e.* no features were observed in the measurements (not shown). This further emphasizes the long-range order which is achieved after preparing the sample in the tilted geometry. These results validate the tilted field geometry conditioning as an effective way to transform the disordered labyrinth domains and resultant sea of skyrmions into an ordered skyrmion lattice. Previous measurements of the Gd/Fe system have reported the skyrmions can locally order into a closed packed lattice.[19, 20] This approach presents a simple procedure to transfer from labyrinth domains to an ordered skyrmion phase, which in this system, remains ordered and stable over an extended temperature and field range.

To further investigate the domain transitions, a projection of the intensity as a function of azimuthal angle, χ (defined in inset of Figure 6), was taken at the peak intensity ($|q| = 0.0025$ Å^{-1} with a $\Delta q = 0.0028$ Å^{-1}). Representative plots for each of the main phases are presented in Figure 6. The transition from the artificial striped domain (solid black squares) to the skyrmion lattice phase (solid red circles) is readily identifiable by the change in the azimuthal pattern from two peaks to the six-peaks; the intensity difference is again attributed to changes in the scattering structure and form factors. We note also that these peaks are separated by 180° and 60°, respectively, identifying the two-fold and regular six-fold patterns in the 2D SANS measurements in Figures 5a and b. The coexistence phase (solid blue circles), which is highlighted at $\mu_0 H$ = -30 mT, (Figure 5c) has a six-fold symmetry with additional intensity at $\chi = 150°$ and 330°; the increase in intensity at these two peaks is consistent with the re-emergence of stripe domains. Approaching magnetic saturation the coexistence phase loses long-range structure, resulting in a collapse in the SANS features into a broad ring, corresponding to an approximately constant intensity of 0.64, at all angles(not shown for clarity) .

The azimuthal projections show that there are regions in the SANS pattern which can be associated with each of the magnetic configurations. Tracking the intensities of these special regions, identified explicitly as circles and squares, in Figure 6, allows us to follow the transitions between the magnetically ordered phases. The field dependence of the scattering intensity from the identified regions (identified in Figure 6 inset), for the [(Fe(3.4 Å)/Gd(4.0 Å)]×120 film stack, is shown in Figure 7a. The intensity of the desig-

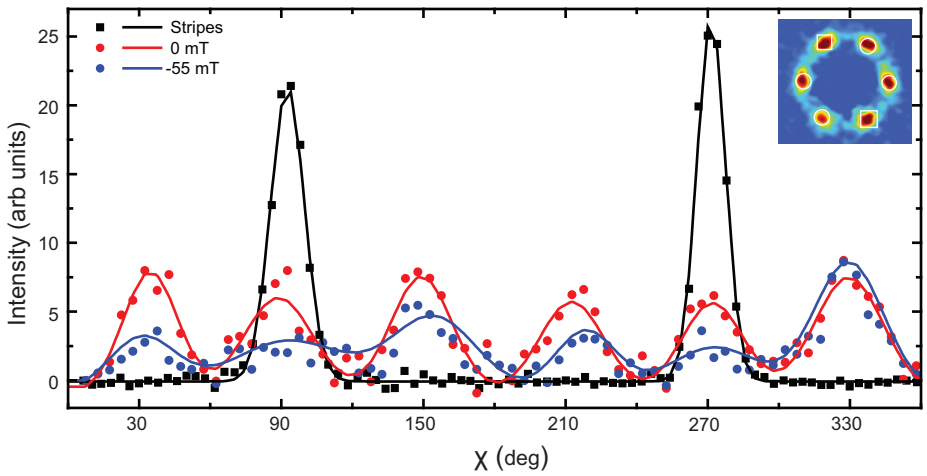

FIG. 6. Azimuthal projection of the intensity for a $q = 0.0025$ Å^{-1} with a $\Delta q = 0.0028$ Å^{-1} for a variety of fields. For $\mu_0 H = 0$ mT (black) after saturation in the tilted geometry,the data shows strong scattering intensity at $\chi = 90°$ and 270°, along the axis of rotation. Increasing the magnetic field to $\mu_0 H = 185$ mT then returning to $\mu_0 H = 0$ mT (red) the azimuthal projection shows a hexagonal pattern with peaks separated by $\approx 60°$ associated with the skyrmion state. Further decreasing the field, (blue) the hexagonal pattern persists with weaker definition, and stronger intensities at $\chi = 150°$ and 330°, indicating the re-emergence of the stripe phase.

nated SANS features is plotted following the field sequence as described above (after saturation in a rotated configuration, return to remanence, rotate to a normal geometry, increase the magnetic field to $\mu_0 H = 185$ mT, then measure under a decreasing magnetic field). The plotted intensity for the ring-like background(blue triangles) and skyrmions(red circles) are as-measured; the intensity of the stripe phase is defined as the measured intensity, minus the skyrmion intensity, plus the background. The calculated stripe phase intensity removes the overlapping skyrmion signal, which includes the ring-like background, then reintroduces the background to allow accurate comparisons to the skyrmion intensity. Tracing the feature associated with the skyrmion phase confirms its stability is robust over a wide range of applied fields, between $\mu_0 H = 185$ mT and $\mu_0 H =$ -30 mT. Passing through remanence the intensity of the skyrmion phase decreases, coinciding with the increase of the stripe phase intensity. The initial increase of the skyrmion phase intensity closely mirrors the increasing intensity of the ring-like background. As noted above, the ring feature corresponds to phases with a common order but no orientation. A likely origin of this feature is therefore

the nucleation of labyrinthine domains, perhaps in regions between skyrmion domains, or in regions of skyrmion-lattice defects.

Temperature scans were collected at 10 K after first preparing the skyrmion state at 300 K with an applied field of $\mu_0 H = 0$ mT. Measuring the scattering intensity as the temperature was increased to 330 K. We observed that the hexagonal SANS pattern was present and unchanging up-to 320 K, at which point it disappeared abruptly. This temperature was identified as the Curie temperature by subsequent magnetization measurements (not shown).

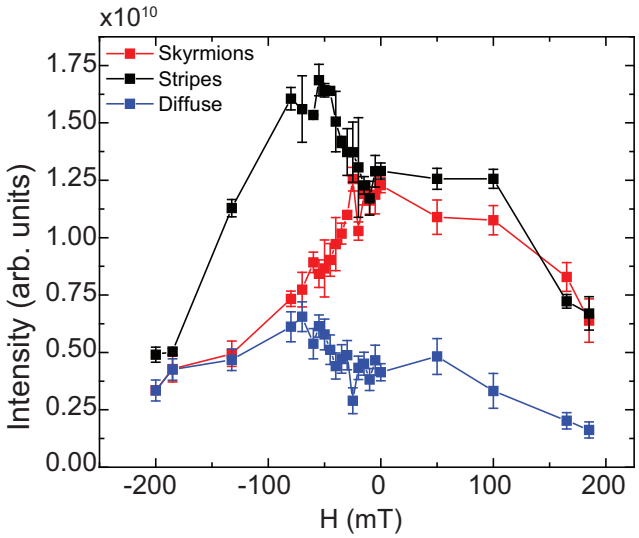

FIG. 7. Scattering intensity from the ring-like background, skyrmion and stripe phases in the [(Fe(3.4 Å) / Gd(4.0 Å)]×120 films are shown as a function of magnetic field. The measurement proceeded from high to low fields (e.g. right to left in the plot).

A key result of the experimentally-observed hexagonal ordering is that these skyrmions possess a mutual repulsive interaction. For Bloch-type skyrmions with random chiralities, and azimuthal-only character, the interaction is not strictly repulsive and skyrmions with opposite chiralities can condense to form biskyrmions which would not form hexagonal arrays[33]. We propose that distortions of the skyrmion structure, in the form of surface-bound flux-closure domains,[19] result in a feature that strengthens the mutual repulsion required to promote lattice ordering. Specifically, in the flux-closure structure, small in-plane domains form at the domain wall/film surface boundary to reduce the stray magnetic fields, shown in Figure 8. The orientation of the domains follow the dipole fields; for a skyrmion with an upward facing core, for example, the dipole fields orient radially outward (away

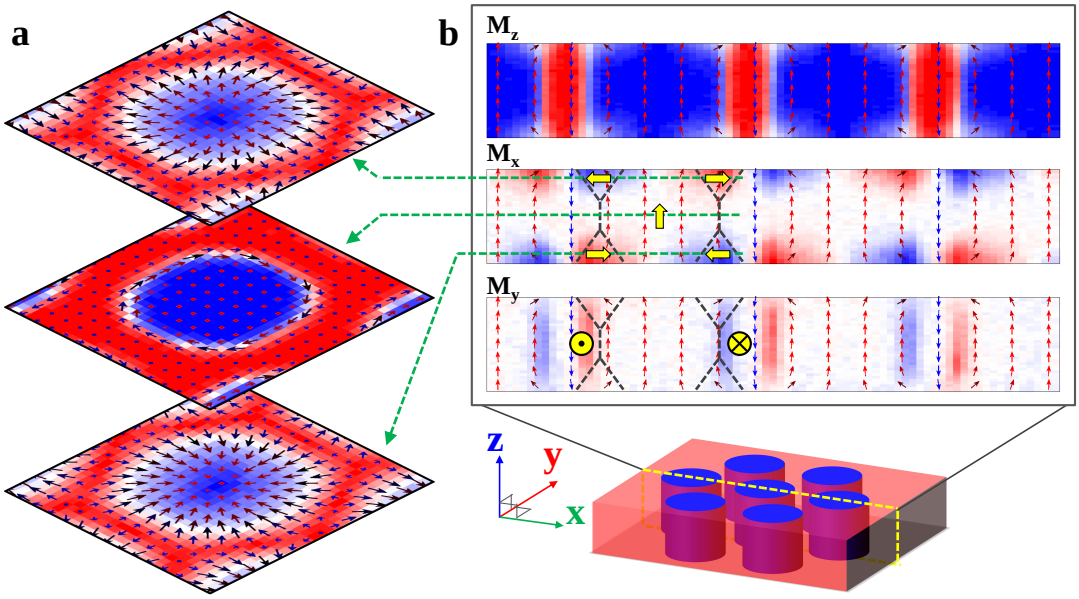

FIG. 8. Micromagnetic simulations of the proposed flux closure skyrmion structure confirm its stability at zero field and a simulated temperature of 300 K. The modeled lattice has skyrmions with a core in the $+z$ direction in a matrix oriented in the $-z$ direction. (**a**) The top-down view shows that the boundary surrounding the core on the top and bottom surfaces are oriented in the radial direction similar to a Néel skyrmion, facing away from the core on the top surface and towards the core on the bottom, following the dipole fields. At the equatorial belt of the skyrmion the moments are oriented along the azimuthal direction, similar to a Bloch structure. (**b**) The cross sectional view of the skyrmion M_z (top) shows the orientation of the core in the +z direction and -z direction of the matrix. The M_x component (middle) confirms the flux closure structure, with the moments on the top and bottom surfaces oriented to follow the dipolar fields. The M_y component (bottom) shows the moments at the barrel of the skyrmion are oriented out of the plane of the page, in opposite directions, due to the bisection of the azimuthally oriented boundary.

from the core) on the top surface, and radially inward (toward the core) on the bottom surface. This proposed structure is similar to a Néel skyrmion structure, but with opposite chiralities on the top and bottom, giving it a net topological charge of zero. However, LTEM results have previously shown that skyrmions in these systems are Bloch-type,[20] with moments oriented in the azimuthal direction, seemingly at odds with the flux-closure structure. In the flux-closure structure, azimuthally-oriented moments would be located at the barrel of the skyrmion between the flux-closure domains; LTEM measurements would

be predominantly sensitive to these azimuthal moments, while the radial moments on the top and bottom would contribute oppositely to the image and thus would tend to cancel out in the transmission geometry, leaving only the Bloch walls. This new hybrid skyrmion construction would possess a net topological charge of unity, with no net contribution from the Néel-type flux-closure caps, and unity from the Bloch-type azimuthally wound moments along the barrel.

To investigate the stability of the described flux closure skyrmion structure inferred from our data, micromagnetic simulations were performed using OOMMF[28] shown in Figure 8. Indeed, the proposed structure was confirmed to be stable at zero field and at simulated temperatures of 300 K. The top-down view of the skyrmions, Figure 8a, shows the moments oriented radially on the top and bottom surfaces, with opposite directions relative to the core, following the dipole fields. At the equatorial belt of the skyrmion, the moments are aligned in the azimuthal direction, consistent with the proposed structure and the LTEM results. The cross-section of the skyrmions, Figure 8b shows that the magnetization follows the proposed flux closure structure, with small surface domains oriented in-plane away from the skyrmion core on the top, and towards the core on the bottom. The magnetization along the y-direction bisects the azimuthal ring, and thus is into the plane on the right, and out of the plane on the left (for the demonstrated counter-clockwise chirality). This specific structure is crucial for the formation of the hexagonal ordering of the skyrmion lattice and has been observed recently in Pt/Co/Ir and Pt/Co/AlO_x multilayers[23]. These simulations did not include RA, and hence demonstrate stability is possible with only dipolar considerations, consistent with previous work[34].

CONCLUSION

We have experimentally demonstrated an approach to generate ordered lattices of hybrid Néel-Bloch skyrmions with long-range order, stable at room temperature and zero applied magnetic field, in amorphous Fe/Gd multilayer thin films. These unique structures were achieved by saturating the film with a tilted magnetic field, facilitating the construction of an ordered stripe phase. This field sequence gives rise to a well ordered state of the skyrmion lattice over a wide range of positive and negative fields ($\approx$ 200 mT), previously unreported, along with a broad range of temperatures (10 K to >320 K). This range of

stability is crucial for the realization of devices stable against stray fields and opperable in a variety of environments. Additionally, these hybrid Néel-Bloch skyrmions lack the in-plane chiral symmetry breaking present in traditional skyrmions stabilized by DM interactions. As a result, both chiralites can exist in these films and can be uniquely controlled, providing additional avenues of manipulation for recording tertiary data-bits, for example. Alternatively, long-range chirality control may be realized within the system by adding additional exchange-coupled layers which possess traditional DM interactions. The ability to stabilize skyrmions at ambient conditions as well as a broad range of fields makes Fe/Gd multilayered thin films ideal candidates for integration into spintronic devices.

ACKNOWLEDGEMENTS

The authors wish to acknowledge the contributions from John Smith (ORNL), Thomas Farmer (ISIS), and Ken Littrell (ORNL). Work at UCSD was supported by the research programs of the U.S. Department of Energy (DOE), Office of Basic Energy Sciences (Award No. DE-SC0003678). Work at the Advanced Light Source, Lawrence Berkeley National Lab (LBNL) was supported by the Director, Office of Science, BES, of the DOE (Contract No. DE-AC02- 05CH11231). Mi-Young Im acknowledges support by the National Research Foundation (NRF) of Korea funded by the Ministry of Education, Science and ICT (2018K1A4A3A03075584, 2016M3D1A1027831, 2017R1A4A1015323) and by the DGIST R&D program of the Ministry of Science, ICT and future Planning (18-BT-02). Access to VSANS was provided by the Center for High Resolution Neutron Scattering, a partnership between the National Institute of Standards and Technology and the National Science Foundation under Agreement No. DMR-1508249. These results use the resources at the High Flux Isotope Reactor, a DOE Office of Science User Facility operated by the Oak Ridge National Laboratory.

---

[1] A. Fert, V. Cros, and J. Sampaio, Skyrmions on the track, Nat. Nanotech. **8**, 152 (2013).

[2] S. Woo, K. Litzius, B.Kruger, M. Im, L. Caretta, K. Richter, M. Man, A. Krone, R. M. Reeve, M. Weigand, P. Agrawal, I. Lemesh, M. A. Mawass, P. Fischer, M. Klaui, and G. S. D. Beach,

Observation of room-temperature magnetic skyrmions and their current-driven dynamics in ultrathin metallic ferromagnets, Nat. Mater. **15**, 501 (2016).

[3] X. Zhang, M. Ezawa, and Y. Zhou, Magnetic skyrmion logic gates: conversion, duplication and merging of skyrmions, Sci. Rep. **5**, 9400 (2015).

[4] W. Jiang, G. Chen, K. Liu, J. Zang, S. G.E. te Velthuis, and A. Hoffmann, Skyrmions in magnetic multilayers, Physics Reports **704**, 1 (2017).

[5] S. Heinze, K. von Bergmann, M. Menzel, J. Brede, A. Kubetzka, R. Wiesendanger, G. Bihlmayer, and S. Blügel, Spontaneous atomic-scale magnetic skyrmion lattice in two dimensions, Nat. Phys. **7**, 713 (2011).

[6] F. Jonietz, S. Mühlbauer, C. Pfleiderer, A. Neubauer, W. Münzer, A. Bauer, T. Adams, R. Georgii, P. Böni, R. A. Duine, K. Everschor, M. Garst, and A. Rosch, Spin transfer torques in mnsi at ultralow current densities, Science **330**, 1648 (2010).

[7] N. Nagaosa and Y. Tokura, Topological properties and dynamics of magnetic skyrmions, Nat. Nanotech. **8**, 899 (2013).

[8] K. Karube, J. S. White, D. Morikawa, M. Bartkowiak, A. Kikkawa, Y. Tokunaga, T. Arima, H. M. Rønnow, Y. Tokura, and Y. Taguchi, Skyrmion formation in a bulk chiral magnet at zero magnetic field and above room temperature, Phys. Rev. Materials **1**, 074405 (2017).

[9] Y. Tokunaga, X. Z. Yu, J. S. White, H. M. Rønnow, D. Morikawa, Y. Taguchi, and Y. Tokura, A new class of chiral materials hosting magnetic skyrmions beyond room temperature, Nature Communications **6**, 7638 (2015).

[10] C. Moreau-Luchaire, C. Moutafs, N. Reyren, J. Sampaio, C. A. F. Vaz, N. Van Horne, K. Bouzehouane, K. Garcia, C. Deranlot, P. Warnicke, P. Wohlhüter, J. M. George, M. Weigand, J. Raabe, V. Cros, and A. Fert, Additive interfacial chiral interaction in multilayers for stabilization of small individual skyrmions at room temperature, Nat. Nanotech. **11**, 444 (2016).

[11] W. Jiang, X. Zhang, G. Yu, W. Zhang, X. Wang, M. Benjamin Jungfleisch, J. E. Pearson, X. Cheng, O. Heinonen, K. L. Wang, Y. Zhou, A. Hoffmann, and S. G. E. te Velthuis, Direct observation of the skyrmion hall effect, Nat. Phys. **13**, 162 (2016).

[12] K. Karube, J. S. White, N. Reynolds, J. L. Gavilano, H. Oike, A. Kikkawa, F. Kagawa, Y. Tokunaga, H. M. Rønnow, Y. Tokura, and Y. Taguchi, Robust metastable skyrmions and their triangularsquare lattice structural transition in a high-temperature chiral magnet, Nat.

Mater. **15**, 1237 (2016).

[13] M. He, L. Peng, Z. Zhu, G. Li, J. Cai, J. Li, H. Wei, L. Gu, S. Wang, T. Zhao, B. Shen, and Y. Zhang, Realization of zero-field skyrmions with high-density via electromagnetic manipulation in pt/co/ta multilayers, Appl. Phys. Lett. **111**, 202403 (2017).

[14] F. Zheng, H. Li, S. Wang, D. Song, C. Jin, W. Wei, A. Kovács, J. Zang, M. Tian, Y. Zhang, H. Du, and R. E. Dunin-Borkowski, Direct imaging of a zero-field target skyrmion and its polarity switch in a chiral magnetic nanodisk, Phys. Rev. Lett. **119**, 197205 (2017).

[15] O. Boulle, J. Vogel, H. Yang, S. Pizzini, D. de Souza Chaves, A. Locatelli, T. Mentes, A. Sala, L. Buda-Prejbeanu, O. Klein, M. Belmeguenai, Y. Roussigne, A. Stashkevich, S. Cherif, L. Aballe, M. Foerster, M. Chshiev, S. Auffret, I. Miron, and G. Gaudin, Room-temperature chiral magnetic skyrmions in ultrathin magnetic nanostructures, Nat. Nanotech. **11**, 449 (2016).

[16] L. Sun, R. Cao, B. Miao, Z. Feng, B. You, D. Wu, W. Zhang, A. Hu, and H. Ding, Creating an artificial two-dimensional skyrmion crystal by nanopatterning, Phys. Rev. Lett. **110**, 167201 (2013).

[17] D. A. Gilbert, B. B. Maranville, A. L. Balk, B. J. Kirby, P. Fischer, D. T. Pierce, J. Unguris, J. A. Borchers, and K. Liu, Realization of ground-state artificial skyrmion lattices at room temperature, Nat. Comun. **6**, 8462 (2015).

[18] B. Dieny, V. S. Speriosu, S. Metin, S. S. P. Parkin, B. A. Gurney, P. Baumgart, and D. R. Wilhoit, Magnetotransport properties of magnetically soft spin-valve structures, J. Appl. Phys. **69**, 4774 (1991).

[19] S. A. Montoya, S. Couture, J. J. Chess, J. C. T. Lee, N. Kent, M. Y. Im, S. D. Kevan, P. Fischer, B. J. McMorran, S. Roy, V. Lomakin, and E. E. Fullerton, Resonant properties of dipole skyrmions in amorphous fe/gd multilayers, Phys. Rev. B **95**, 224405 (2017).

[20] S. A. Montoya, S. Couture, J. J. Chess, J. C. T. Lee, N. Kent, D. Henze, S. K. Sinha, M. Y. Im, S. D. Kevan, P. Fischer, B. J. McMorran, V. Lomakin, S. Roy, and E. E. Fullerton, Tailoring magnetic energies to form dipole skyrmions and skyrmion lattices, Phys. Rev. B **95**, 024415 (2017).

[21] E. M. Chudnovsky and D. A. Garanin, Skyrmion glass in a 2d heisenberg ferromagnet with quenched disorder, New J. Phys. **20**, 033006 (2018).

[22] H. A. Dürr, E. Dudzik, D. S., J. B. Goedkoop, G. van der Laan, M. Belakhovsky, C. Mocuta, A. Marty, and Y. Samso, Chiral magnetic domain structures in ultrathin fepd films, Science **284**, 5423 (1999).

[23] W. Legrand, J.-Y. Chauleau, D. Maccariello, N. Reyren, S. Collin, K. Bouzehouane, N. Jaouen, V. Cros, and A. Fert, Hybrid chiral domain walls and skyrmions in magnetic multilayers, Science Advances **4** (2018).

[24] I. Lemesh and G. S. D. Beach, Twisted domain walls and skyrmions in perpendicularly magnetized multilayers, Physical Review B **98**, 104402 (2018).

[25] R. K. Dumas, D. A. Gilbert, N. Eibagi, and K. Liu, Chirality control via double vortices in asymmetric co dots, Phys. Rev. B **83**, 060415 (2011).

[26] W. T. Heller, M. Cuneo, L. Debeer-Schmitt, C. Do, L. He, L. Heroux, K. Littrell, S. V. Pingali, S. Qian, C. Stanley, V. S. Urban, B. Wu, and W. Bras, The suite of small-angle neutron scattering instruments at oak ridge national laboratory, Journal of Applied Crystallography **51**, 242 (2018).

[27] G. D. Wignall, K. C. Littrell, W. T. Heller, Y. B. Melnichenko, K. M. Bailey, G. W. Lynn, D. A. Myles, V. S. Urban, M. V. Buchanan, D. L. Selby, and P. D. Butler, The 40m general purpose small-angle neutron scattering instrument at Oak Ridge National Laboratory, Journal of Applied Crystallography **45**, 990 (2012).

[28] M. J. Donahue, *OOMMF user's guide, version 1.0*, Tech. Rep. (National Institute of Standards and Technology, 1999).

[29] P. Milde, D. Köhler, J. Seidel, L. M. Eng, A. Bauer, A. Chacon, J. Kindervater, S. Mühlbauer, C. Pfleiderer, S. Buhrandt, C. Schütte, and A. Rosch, Unwinding of a skyrmion lattice by magnetic monopoles, Science **340**, 1076 (2013).

[30] F. Hellman, E. Abarra, A. Shapiro, and R. Van Dover, Specific heat of amorphous rare-earth–transition-metal films, Physical Review B **58**, 5672 (1998).

[31] See supplemental material at [url will be inserted by publisher] for more x-ray data.

[32] S. Mühlbauer, B. Binz, F. Jonietz, C. Pfleiderer, A. Rosch, A. Neubauer, R. Georgii, and P. Böni, Skyrmion lattice in a chiral magnet, Science **323**, 915 (2009).

[33] J. C. T. Lee, J. Chess, S. A. Montoya, X. Shi, N. Tamura, S. K. Mishra, D. H. Parks, P. Fischer, B. McMorran, S. K. Sinha, E. E. Fullerton, S. D. Kevan, and S. Roy, Synthesizing skyrmion bound pairs in fe-gd thin films, Applied Physics Letters **109**, 022402/1 (2016).

[34] F. Büttner, I. Lemesh, and G. S. Beach, Theory of isolated magnetic skyrmions: From fundamentals to room temperature applications, Scientific reports **8**, 4464 (2018).